PAPER

Brightening of a supersonic beam of neutral atoms

IOP Publishing Physica Scripta
Phys. Scr. 93 (2018) 124009 (5pp) https://doi.org/10.1088/1402-4896/aae716

Brightening of a supersonic beam of neutral atoms

E Anciaux, G Stratis and M G Raizen

Department of Physics and Center for Nonlinear Dynamics, University of Texas at Austin, Austin, TX, United States of America

E-mail: anciaux.erik@gmail.com

Received 17 July 2018, revised 10 September 2018
Accepted for publication 10 October 2018
Published 31 October 2018

Abstract

Well-collimated, high-intensity beams of neutral atoms have many applications ranging from atom microscopy to atom interferometry to ultracold atomic physics. We experimentally demonstrate a method for brightening a supersonic atomic beam and observe an increase in the phase space density by a factor of at least 20. Our scheme relies upon a permanent magnetic hexapole lens to focus a divergent beam of neutral atoms emitted from a supersonic nozzle and transverse laser cooling as the beam converges downstream from the lens so as to create a dense, narrow, Doppler-collimated atomic beam. In principle, this method can be repeated multiple times in series for further beam brightening.

Keywords: magnetic hexapole, beam brightening, supersonic beam, atomic focusing, laser cooling

(Some figures may appear in colour only in the online journal)

1. Introduction

This paper is in honor of the 60th birthday of Wolfgang Schleich, a long-standing friend and colleague who has made many contributions to physics. As someone who has played a leading role as a theorist in the development of new tools to control and cool atoms, this paper on brightening of supersonic beams should be of interest to Wolfgang, and we hope that it stimulates more ideas and proposals. The ability to control and cool atoms in the gas phase has been enabled by the method of laser cooling which produces ultra-cold atomic gases [1–3]. These atoms are then further cooled by evaporation, creating Bose–Einstein condensates and the so-called atom laser [4, 5]. Current applications of atoms in technology include atomic clocks for the global positioning system, atomic interferometry for inertial navigation and remote sensing, atomic magnetometers for medicine, and ion beams for microscopy and nanofabrication [6–12]. The two major limitations of laser cooling have been generality and flux, and we have been working on a new set of methods to overcome these limitations [13]. These include magnetic stopping of supersonic beams and further cooling by a one-way wall for atoms, realizing the historic thought experiment of Maxwell's demon [14]. This is a crucial component in optical and electron imaging, providing diffraction-limited resolution. In this paper, we introduce and characterize a new addition to our toolbox: a method for brightening of supersonic beams, which combines magnetic focusing with the proven brightening method of transverse laser cooling, creating a significantly brighter beam than could be achieved through cooling alone [15, 16] while significantly decreasing the often impractically long laser interaction times and high laser powers inherent in 2D MOTs [17–19]. Such beam brightening was proposed for effusive atomic beams, but never realized in practice [1]. We first provide a general schematic of the set-up, and describe in details the results of our beam brightening apparatus. Recent work by our group on a pulsed magnetic hexapole offers a solution to correct for chromatic aberration inherent in imaging beams with nonzero temperature. When used in conjunction with the beam brightening methods discussed in this paper, this aberration-correction should enable the development of a neutral atom microscope with atomic resolution [20, 21] without relying on flux limiting elements such as apertures or Fresnel zone plates common in present day neutral atom microscopy [22–26].

2. Beam brightening apparatus

We create a supersonic beam of neutral metastable neon atoms using a pulsed trumpet-shaped nozzle and dielectric barrier discharge attachment which excites a fraction 10^{-4} of

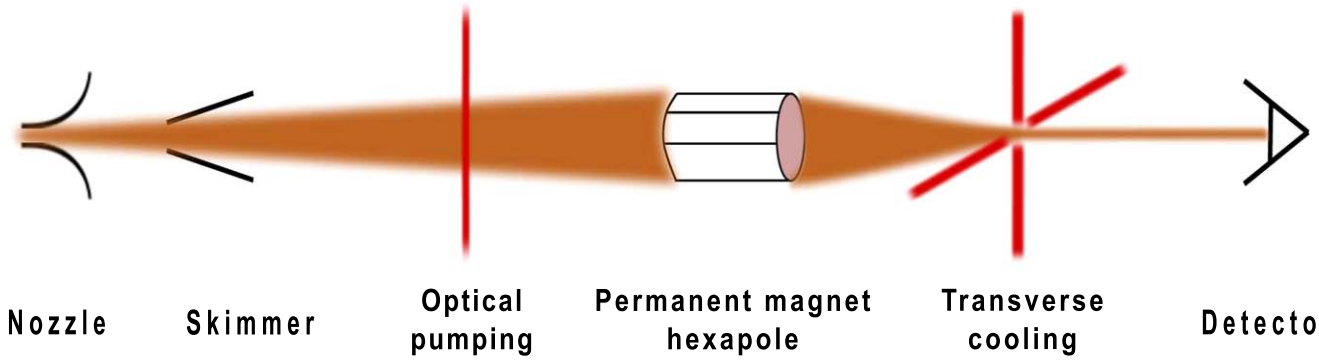

Figure 1. Schematic illustration of experimental beamline. A supersonic beam of metastable neon atoms is optically pumped to a low-field-seeking state and passes through a permanent magnetic hexapole lens which images the beam toward a plane at which the beam is collimated using transverse cooling. The beam then propagates toward an MCP with phosphor screen.

the beam to a metastable paramagnetic $^3P_2$ state. The supersonic beam then passes through a 5 mm diameter skimmer 20 cm downstream from the nozzle. We then optically pump the beam to a low field seeking $m_j = 2$ magnetic state.

The beam propagates 20 cm towards and through a permanent magnetic hexapole lens which images the beam to a plane 22 cm downstream from the center of the magnetic lens. It is then transverse laser cooled to near the Doppler limit and propagates 102 cm to a micro-channel plate (MCP) with phosphor screen that serves as a detector. All laser cooling interactions rely upon a 640 nm injection locked diode laser to excite the $^3P_2 \rightarrow ^3 D_3$ transition. All laser detunings necessary for laser cooling are created using acousto-optic modulators. A schematic illustration of the brightening apparatus is shown in figure 1.

3. Permanent magnetic hexapole lens

The permanent magnetic lens consists of six sets of permanent magnets with orientation and magnetic field as shown in figure 2. Each set of magnets is rotated 60° from the previous set and has alternating inward–outward polarization.

The magnets are held in six trenches in a 7.6 cm long cylindrical delrin block. A titanium tube passing through the center of the block serves as the vacuum chamber for this section of the beamline and is coupled to the remainder of the vacuum system using rubber o-rings. The axis of the lens is collinear with the nozzle and skimmer.

Over the region defined by $\rho < a/2$, where ρ is the radial position, a is the distance from the lens axis to the inside of the permanent magnets, and ϕ is the angle from the x-axis, the magnetic field profile can be approximated by the formula

$$\mathbf{B} \approx B_0 \frac{\rho^2}{a^2}(\sin(2\phi)\hat{x} + \cos(2\phi)\hat{y}). \quad (1)$$

B_0 is given by the magnetization of the permanent magnets multiplied by the filling fraction. The filling fraction is the proportion of the circumference of the circle defined by the inner edges of the permanent magnets which is filled by the permanent magnets. In our case, the magnetization of each magnet is 1.45 T and the filling fraction is $\frac{1}{\pi}$ giving a final value for B_0 of 0.462 T.

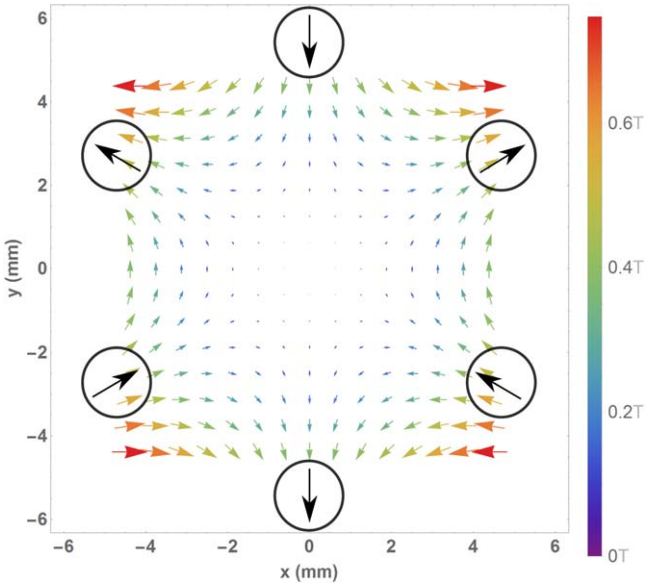

Figure 2. Permanent magnetic hexapole orientation and magnetic field.

An atom traveling through an inhomogeneous magnetic field experiences a force proportional to the gradient of the magnitude of the magnetic field. The direction is given by the magnetic quantum number m_j. For the case of neon atoms in the metastable $^3P_2$ state with magnetic quantum number $m_j = 2$, atoms will feel a force in a direction of decreasing magnetic field strength, hence why it is referred to as a low-field-seeking state.

$$\mathbf{F} = -m_j g_j \mu_B \nabla |\mathbf{B}|, \quad (2)$$

where $g_j \approx \frac{3}{2}$ is the Landé g factor and μ_B is the Bohr magneton.

Inside the bore of the permanent magnetic hexapole lens, atoms will feel a force towards the axis of the lens

$$\mathbf{F} \approx -B_0 \frac{2}{a^2} m_j g_j \mu_B \boldsymbol{\rho} \approx -1.13 \times 10^{-18}\,\mathrm{N/m}\,\boldsymbol{\rho}. \quad (3)$$

The linear relationship between force on low field seeking atoms and radial distance gives the permanent magnetic hexapole its lens-like properties. Atoms passing through the lens will feel a total impulse proportional to their radial distance and time spent in the lens and thus the length of the lens itself, creating an

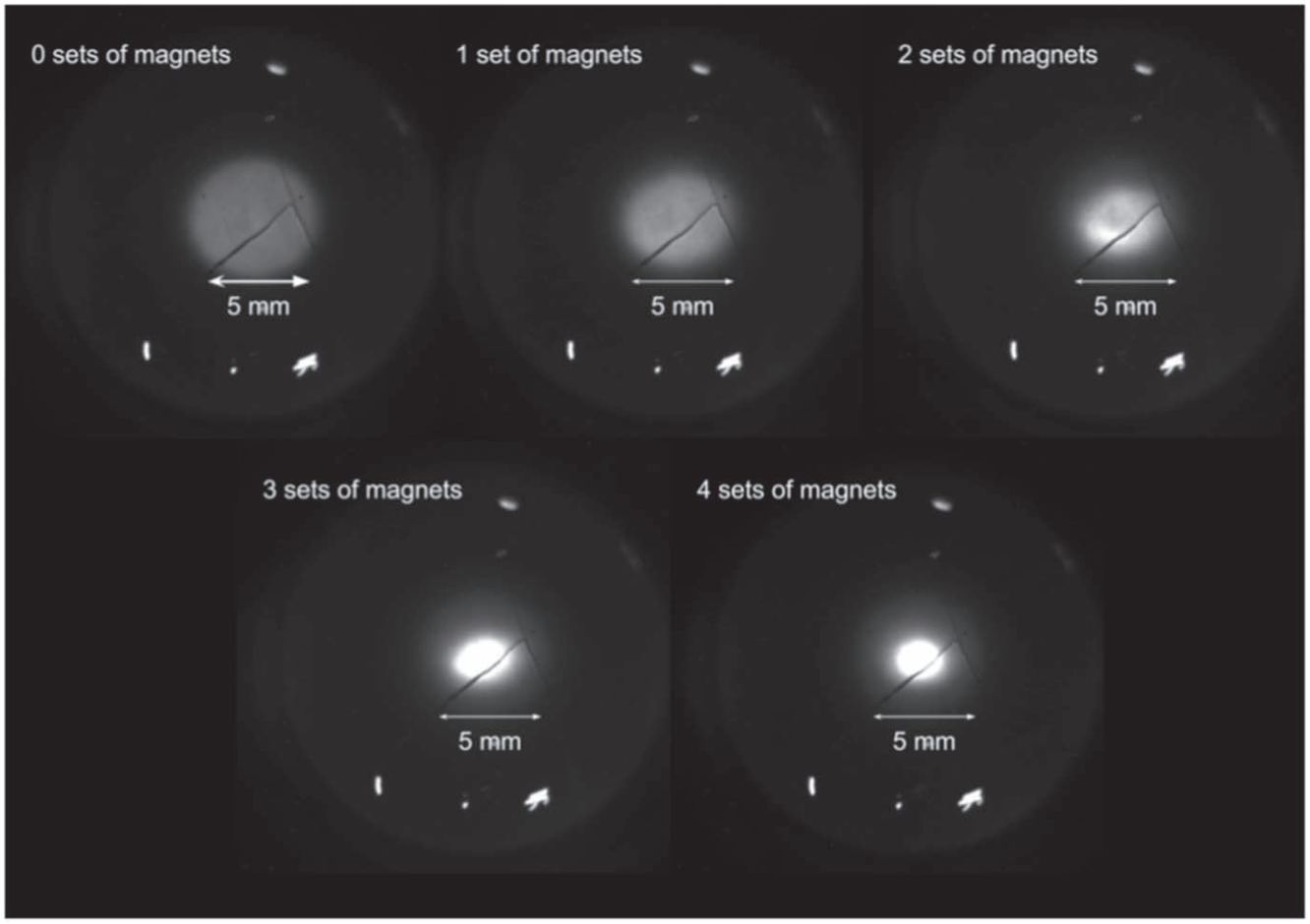

Figure 3. CCD images of a supersonic atomic beam on an MCP as the beam is brought into focus by increasing the power of a permanent magnetic hexapole lens. The crack in the MCP does not affect the measured results.

effective focal length that is independent of initial radial position and inversely proportional to the length of the lens. For an average longitudinal velocity $v_{\|} \approx 490\ \mathrm{m\ s^{-1}}$ and lens length 7.6 cm, we estimate a focal length of $f \approx 9.3$ cm.

4. Magnetic hexapole results

To test the performance of the permanent magnetic lens, we use an MCP to detect the beam at a plane 22 cm downstream from the lens. Starting from zero magnets in our delrin mount, we lengthen our magnetic hexapole lens by integer multiples of 1.9 cm corresponding to the length of a single magnet. We then image the beam on the detector with a charge-coupled device camera, the results of which are shown in figure 3.

Without any magnets in the mount, the atomic beam passes unfocused through the magnetic lens and has a full width half maximum (FWHM) diameter of 6.4 mm. As magnets are added so as to increase the length of the magnetic lens to 7.6 cm, the beam diameter decreases to a minimum FWHM of 1.5 mm. The detected peak flux increases by a factor of 12 from roughly 10^{12} to $10^{13}\ \mathrm{cm^{-2}\ s^{-1}}$ as shown in figure 4. This dense and narrow but divergent beam serves as a starting point for laser cooling.

5. Beam brightening via laser cooling

Beam brightness is measured in terms of transverse phase space density, the number of atoms, n per unit area, A per unit solid divergence angle, Ω,

$$B = \frac{\mathrm{d}n}{\mathrm{d}A\mathrm{d}\Omega}. \tag{4}$$

While the permanent magnetic lens increases the density of the atomic beam, it does not increase the beam brightness. It converts a reasonably well collimated, but wide beam into a well focused beam with a large divergence angle at its narrowest point. The focusing from the magnetic lens increases the maximum brightness that can be achieved through laser cooling, but the increase in phase space density of the system comes exclusively from laser cooling.

Two limits to consider are the capture limit and the Doppler-limited divergence angle. The ratio of the atomic beam divergence to the capture limit sets the proportion of the atomic beam which can be brightened while the Doppler-limited divergence angle is the minimum beam divergence we can achieve through laser cooling. The capture limit is determined by the detuning of the lasers used for transverse cooling. We use a detuning equal to the natural linewidth of the $^3P_2 \rightarrow {}^3D_3$ transition, 8.18 MHz, which corresponds to a velocity of

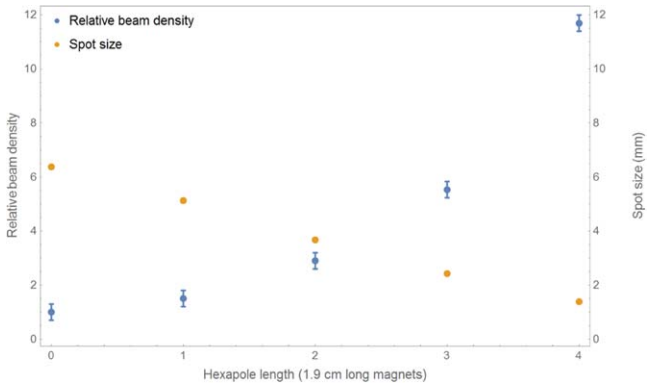

Figure 4. The relative beam density and spot size (FWHM) of the atomic beam as magnets are added to the magnetic hexapole lens.

5.1 m s^{-1}. We can geometrically estimate the largest transverse velocity of atoms within the beam at the collimation region, $v_{\max} \approx \frac{\rho_{\max}}{i} v_{\|} \approx 5.0$ m s^{-1}, where $\rho_{\max}$ is the maximum radial position within the lens defined by the inner diameter of the lens and i is the propagation distance from the magnetic lens to the MCP. This maximum transverse velocity is within the capture region and can thus be collimated by standard methods of transverse cooling.

The Doppler limit is the minimum velocity distribution width that can be achieved through laser cooling, which for metastable neon is 28.5 cm s^{-1}. This corresponds to a divergence angle of 0.58 mrad. As we use FWHM for our measurements, it is also convenient to consider the Doppler limit and divergence angle in terms of FWHM. They are 67 cm s^{-1} and 1.37 mrad respectively.

The Doppler limit is defined based on a detuning of half the linewidth, while we are using a detuning equal to a full linewidth so as to increase our capture range. The minimum velocity distribution width we can achieve with this detuning is 34.9 or 82.2 cm s^{-1} FWHM. This corresponds to a divergence angle of 1.68 mrad FWHM.

6. Beam brightening results

To estimate the brightness of the atomic beam as it leaves the brightening apparatus, we first need to measure its divergence angle. To do this, we employ a two point measurement, with one point at the laser cooling region and one point 102 cm downstream. The beam expands from a FWHM of 1.5 mm to a FWHM of 3.4 mm over the course of 102 cm corresponding to an angle of 1.86 mrad FWHM. This corresponds to beam with an estimated brightness of 10^{19} s^{-1} cm^{-2} sr^{-1}. The measured camera pixel brightness and therefore atomic beam density increases by a factor of 36 higher when the beam is focused and brightened as compared to the baseline case of no focusing and brightening as shown in figure 5, however this should not be confused with an increase in beam brightness as the brightened and non-brightened beams do not have the same divergence angle as they reach the detector.

To more accurately estimate the brightness increase from our scheme, we standardize the width of the beam at the first point of a two point measurement by adding a 100 μm slit 15 cm downstream from the laser cooling region. We compare the peak beam densities of both a focused and brightened beam and a non-brightened beam on a detector 87 cm downstream from the slit. We know through geometric arguments that transverse positions on the detector are nearly perfectly correlated with transverse angle, as all atoms in the beam originate at approximately the same transverse position defined by the slit, therefore the increase in beam brightness will be proportional to the increase in peak beam density, measured to be a factor of 21 as shown in figure 6 and will not depend on the width of the measured beam.

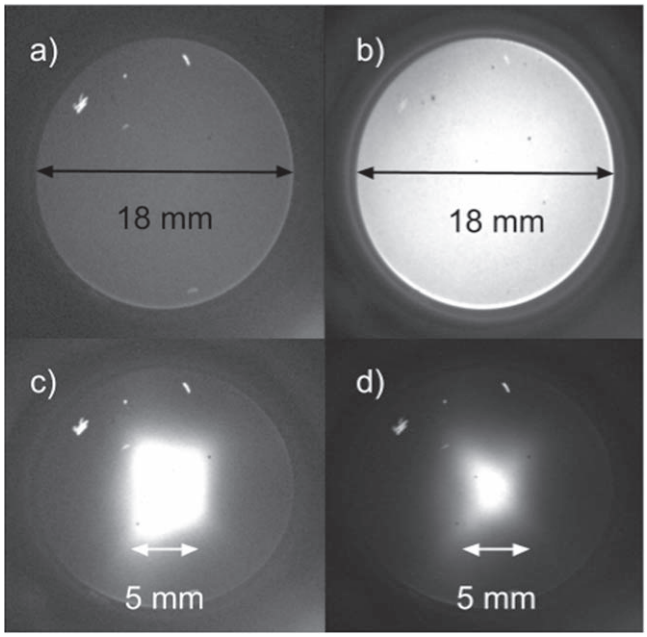

Figure 5. CCD images of a metastable atomic beam impinging on an MCP with phosphor screen 102 cm downstream from the laser cooling region. Adding our beam brightening apparatus increases the detected beam density by a factor of 36 and decreases the spot size from 7.8 to 3.4 mm. (a) Non-brightened beam. (b) Non-brightened beam with increased MCP gain for image clarity. (c) Brightened beam with the same MCP gain as shown in (a). (d) Brightened beam with reduced gain for clarity.

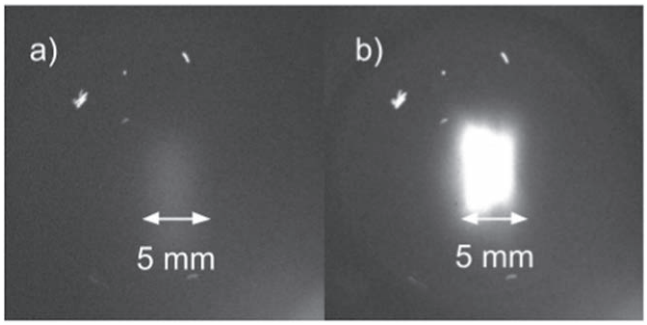

Figure 6. CCD images of a metastable atomic beam impinging on an MCP with phosphor screen 87 cm downstream from a 100 μm slit. The peak beam density and therefore peak beam brightness increases by a factor of 21. (a) Non-brightened beam through a slit. (b) Brightened beam through a slit.

7. Conclusion

We have introduced a novel mechanism for brightening a supersonic beam of neutral metastable neon atoms. Our scheme uses a permanent magnetic hexapole as a lens to focus an atomic beam to a spot size as low as 1.5 mm FWHM with an estimated beam density of 10^{13} s^{-1} cm^{-2}. We then brighten the beam at its narrowest point using standard methods of transverse cooling, achieving an estimated beam brightness of 10^{19} s^{-1} cm^{-2} sr^{-1}, an increase in brightness by a factor of 21. In principle, our scheme can be repeated in series with a chain of aberration-corrected magnetic lenses [21] and transverse cooling beams so as to further focus and brighten an atomic beam to an estimated limit of up to 10^{24} s^{-1} cm^{-2} sr^{-1} corresponding to both a Doppler limited divergence angle and Penning ionization limited atomic density.

Acknowledgments

The authors thank Dr Jamie Gardner for helpful comments on the manuscript as well as Jordan Zesch and Zoe de Beurs for assistance with the experiments. We acknowledge the support of the RA Welch Foundation Grant No. F-1258, the National Science Foundation Grant No. PHY-1704059, and the Sid W Richardson Foundation.

References

[1] Metcalf H and van der Straten P 1999 *Laser Cooling* (Berlin: Springer)
[2] Wineland D, Drullinger H and Walls F 1978 Radiation-pressure cooling of bound resonant absorbers *Phys. Rev. Lett.* **40** 1639–42
[3] Kasevich M and Chu S 1992 Laser cooling below a photon recoil with three level atoms *Phys. Rev. Lett.* **69** 1741–4
[4] Ketterle W 2002 Nobel lecture: when atoms behave as waves: Bose–Einstein condensation and the atom laser *Rev. Mod. Phys.* **74** 1131
[5] Bolpasi V, Efremidis N K, Morrissey M J, Condylis P C, Sahagun D, Baker M and von Klitzing W 2014 An ultra-bright atom laser *New J. Phys.* **16** 033036
[6] Ludlow A D, Boyd M M, Ye J, Peik E and Schmidt P O 2015 Optical atomic clocks *Rev. Mod. Phys.* **87** 637–701
[7] Cronin A D, Schmiedmayer J and Pritchard D E 2009 Optics and interferometry with atoms and molecules *Rev. Mod. Phys.* **81** 1051–129
[8] Hamilton P, Jaffe M, Brown J, Maisenbacher L, Estey B and Müller H 2015 Atom interferometry in an optical cavity *Phys. Rev. Lett.* **114** 100405
[9] Shah V, Knappe S, Schwindt P D D and Kitching J 2007 Subpicotesla atomic magnetometry with a microfabricated vapour cell *Nat. Photon.* **1** 649–52
[10] Hanssen J L, McClelland J J, Dakin E A and Jacka M 2006 Laser-cooled atoms as a focused ion beam source *Phys. Rev. A* **74** 063416
[11] Harada Y, Masuda S and Ozaki H 1997 Electron spectroscopy using metastable atoms as probes for solid surfaces *Chem. Rev.* **97** 1879–952
[12] Joens M S 2013 Helium ion microscopy (HIM) for the imaging of biological samples at sub-nanometer resolution *Sci. Rep.* **3** 3514
[13] Raizen M, Budker D, Rochester S, Narevicius J and Narevicius E 2014 Magneto-optical cooling of atoms *Opt. Lett.* **39** 4502–5
[14] Raizen M G 2009 Comprehensive control of atomic motion *Science* **324** 1403–6
[15] Joffe M A, Ketterle W, Martin A and Pritchard D E 1993 Transverse cooling and deflection of an atomic beam inside a Zeeman slower *J. Opt. Soc. Am.* B **10** 2257–62
[16] Leefer N, Cingoz A, Gerber-Siff B, Sharma A, Torgerson J R and Budker D 2010 Transverse laser cooling of a thermal atomic beam of dysprosium *Phys. Rev.* A **81** 043427
[17] Riis E, Weiss D S, Moler K A and Chu S 1990 Atom funnel for the production of a slow, high-density atomic beam *Phys. Rev. Lett.* **64** 1658–61
[18] Nellessen J, Werner J and Ertmer W 1990 Magneto-optical compression of a monoenergetic sodium atomic beam *Opt. Commun.* **78** 300–8
[19] Swanson T B, Silva N J, Mayer S K, Maki J J and McIntyre D H 1996 Rubidium atomic funnel *J. Opt. Soc. Am.* B **13** 1833–6
[20] Castillo-Garza R, Gardner J R, Zisman S and Raizen M G 2013 Nanoscale imaging of neutral atoms with a pulsed magnetic lens *ACS Nano* **7** 4378–83
[21] Gardner J R, Anciaux E M and Raizen M G 2017 Neutral atom imaging using a pulsed electromagnetic lens *J. Chem. Phys.* **146** 081102
[22] Witham P J and Sánchez E J 2012 Increased resolution in neutral atom microscopy *J. Microsc.* **248** 223–7
[23] Barr M, Fahy A, Jardine A, Ellis J, Ward D, MacLaren D A, Allison W and Dastoor P C 2014 A design for a pinhole scanning helium microscope *Nucl. Instrum. Methods Phys. Res.* B **340** 76–80
[24] Barr M, Fahy A, Martens J, Jardine A P, Ward D J, Ellis J, Allison W and Dastoor P C 2016 Unlocking new contrast in a scanning helium microscope *Nat. Commun.* **7** 10189
[25] Koch M, Rehbein S, Schmahl G, Reisinger T, Bracco G, Ernst W E and Holst B 2008 Imaging with neutral atoms: a new matter-wave microscope *J. Microsc.* **229** 1–5
[26] Eder S D, Reisinger T, Greve M M, Bracco G and Holst B 2012 Focusing of a neutral helium beam below one micron *New J. Phys.* **14** 073014